IEEE Access
Multidisciplinary | Rapid Review | Open Access Journal

Received December 14, 2016, accepted December 29, 2016, date of publication January 10, 2017, date of current version March 8, 2017.

Digital Object Identifier 10.1109/ACCESS.2017.2651113

On-Line Stator Open-Phase Fault Detection and Tolerant Control for Permanent Magnet Machines Using the Neutral Point Voltage

SHIH-CHIN YANG, (Member, IEEE), GUAN-REN CHEN, (Student Member, IEEE), AND DA-REN JIAN

National Taiwan University, Taipei 10617, Taiwan

Corresponding author: S.-C. Yang (scy99@ntu.edu.tw)

ABSTRACT Conventional machine stator open-phase fault detection methods rely on the detection of current harmonics from the sensing of phase currents. Because the magnitudes of current harmonics are proportional to the machine load condition, it is a challenge for the phase fault detection at the light load condition when fault-induced current harmonics are too small to detect. This paper proposes an improved stator phase fault detection for permanent magnet (PM) machines based on the use of neutral point (NP) in Y-connected windings. It is shown that the first-order voltage harmonic is resultant once the open-phase fault occurs. Comparing with prior detection methods based on the current measurement, the fault detection using NP voltage is insensitive to the load condition, because the proposed fault signal is induced by the voltage unbalance as a result of the open phase. In addition, considering the fault tolerant control, a single-phase drive is developed by connecting the machine NP to one of the inverter legs. The machine can drive at the most efficient condition using standard three-leg inverters under phase fault. A 50-W PM machine with the accessible NP is used to evaluate the proposed open-phase fault detection and tolerant control method.

INDEX TERMS Motor condition monitoring, motor fault detection, fault tolerant control.

I. INTRODUCTION

Variable-frequency PM machine drives are applied in applications ranging from small fans and compressors to the large transportation systems. For the implementation of variable-frequency drives, high efficient real-time microcontrollers with advanced machine drive algorithms are typically used to control semiconductor switches and generate pulse-width-modulation (PWM) voltages. Due to the progress on the microcontroller, on-line condition monitoring and fault tolerant control can also be implemented by using the microcontroller as the fault monitor [1], [2]. For example, an adaptive controller is designed to detect faults in active suspension system [3]. A fault tolerant control is also developed to mitigate unknown actuator faults in the same system [4]. A nonlinear controller is implemented to improve the reliability in a hydraulic rotary actuator [5].

PWM inverter faults are one of the main fraction of overall machine drive faults, which can account for up to 38% in industrial drives [6]. Among these faults, open-phase fault typically appears when either one phase of the machine or inverter switch leg is completely disconnected. This type of fault might not suddenly result in circulating currents in the inverter to trigger the over-current protection. However, if machines continuously drive under this fault condition, secondary failures could be induced in the inverter or machine due to high torque ripples and rotor vibrations [7].

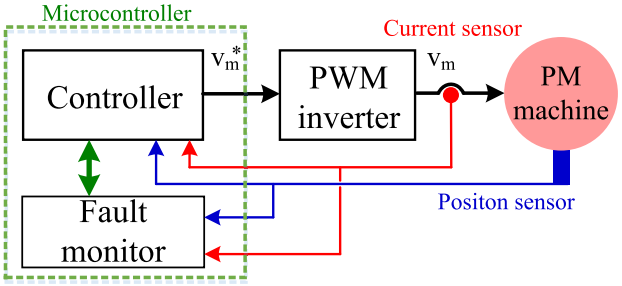

FIGURE 1. On-line fault detection using the microcontroller in the machine drive.

Several fault detection methods have been developed for the open-phase fault. To achieve on-line fault detection performance, machine drive available current or position signal shown in Fig. 1 can be used to develop a fault monitor. Depending on the signal process of estimated fault signal,

these detection techniques can be categorized into frequency-domain methods [8], [9] and time-domain methods [10]–[12]. For frequency-domain methods, the harmonic spectrum of current or position is calculated at least one electrical cycle. With the knowledge of harmonic location, the fault induced harmonic can be extracted to design the fault indicator. However, considering the implementation of on-line fault detection, the fault harmonic spectrum can only be estimated when the drive is operated at steady state. It is important to note that the phase fault is primarily resulted from the open transistor, inappropriate gate signals or open connector during the change of speed and torque load. Under this effect, frequency-domain methods might not be useful for variable-frequency drives with the dynamic operation.

On the other hand, the phase fault detection based on time-domain methods are able to identify the fault during speed and load transient. Considering a healthy machine drive, dq currents should be constant values with field oriented control (FOC). Once the phase fault occurs, visible second-order harmonics are induced in dq currents. By measuring machine phase currents in Fig. 1, the phase fault can be found based on the calculation of d- and q-axis current [11]. In general, the fault detection using the time-domain method can find a phase fault within a second in variable-frequency drives. However, current measurement noises and inverter dead-time harmonics result in the distortion on dq currents, limiting the fault detection performance [13]. Under this effect, the threshold of fault indictor should be designed experimentally for different machines drives with different parameters [14].

After detecting a machine fault, a reliable post-fault operation can also be implemented in variable-frequency drives. These fault tolerant systems are typically implemented based on additional switches [15], additional phases [16] or a fourth inverter leg [17], [18] on an inverter. In general, integrated power modules consisting of six switches are typically used to implement PWM control in a standard inverter. For conventional tolerant systems with redundant devices, special inverter topologies instead of power modules must be used to have fault-tolerant capabilities. Although the comparable drive performance can be achieved for the operation with the phase fault, significant system costs on these special inverters might result, e.g. 115% cost on the standard inverter for a four leg inverter [19].

This paper proposes an on-line stator phase fault detection and tolerant control for PM machines. The machine NP is used for both the phase fault detection and post-fault tolerant control. Based on the analysis of machine NP model, a first-order harmonic with respect to the rotor frequency is induced in the NP voltage once phase fault appears. Because the fault harmonic in the NP voltage is induced only by the voltage unbalance, the proposed fault detection should be insensitive to the parameter variation during the load changes. Considering the application on variable-frequency drives, a time-domain method is developed to isolate this phase fault induced NP voltage harmonic for the monitoring. According to the experimental evaluation, the phase fault can be detected during speed and load transient using the proposed detection method.

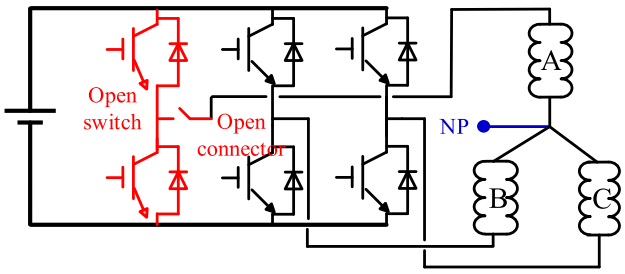

FIGURE 2. PM machine drive with the phase fault in A-phase.

For the tolerant control, the proposed NP can also be connected to one leg of inverter to achieve the single-phase machine operation during the presence of phase fault. Compared to prior redundant designs in [15]–[19], the proposed tolerant control is implemented on the standard three-phase inverter. Only two single-pole double-throw (SPDT) switches are added to convert the three-phase drive to the single-phase drive. A faulty machine is able to operate at the most efficient condition using the standard inverter. A 50-W PM machine with the proposed NP is tested to evaluate the proposed open-phase fault detection and tolerant control.

II. PM MACHINE MODEL CONSIDERING THE PHASE FAULT

This section analyzes the NP voltage response with the influence of open phase fault. Figure 2 illustrates the PM machine drive with the open-phase on A-phase. This type of fault typically occurs due to the open circuit in the machine cable connector or one inverter leg. A time-domain detection method will be developed to isolate the fault signal in the measured NP voltage.

A. NP VOLTAGE IN A HEALTHY MACHINE

Considering firstly a healthy machine, the corresponding three-phase line-to-neutral voltages can be modelled by

$$\begin{aligned} V_{s\_NP} &= R_s I_s + L_s \frac{dI_s}{dt} + I_s \frac{dL_s}{dt} + \frac{d\lambda_{pm}}{dt} \\ &\approx R_s I_s + j\omega_e L_s I_s + j\omega_e \lambda_{pm} \end{aligned} \quad (1)$$

In (1), the machine resistance, R_s, and inductance, L_s, are assumed as constants for simplicity. The derivative term of $\frac{dI_s}{dt}$ is equal to $j\omega_e I_s$ considering the current response at steady-state where ω_e is the rotor frequency. In addition, V_{s_NP}, I_s and λ_{pm} represent three-phase voltages, currents and fluxes matrices which are respectively shown by

$$\begin{aligned} V_{s\_NP} &= \begin{bmatrix} v_{a\_NP} & v_{b\_NP} & v_{c\_NP} \end{bmatrix}^T \\ &= \begin{bmatrix} v_a - v_{NP} & v_b - v_{NP} & v_c - v_{NP} \end{bmatrix}^T \quad (2) \\ I_s &= \begin{bmatrix} i_a & i_b & i_c \end{bmatrix} \quad (3) \\ \lambda_{pm} &= \begin{bmatrix} \lambda_{pma} & \lambda_{pmb} & \lambda_{pmc} \end{bmatrix} \quad (4) \end{aligned}$$

Here, the subscripts "a," "b" and "c" represent the voltage and current quantity in A-, B- and C-phase of the machine,

the subscript "NP" denotes the voltage in NP, and the subscript "pma," "pmb" and "pmc" are the PM flux in three phases. For Y-connected machine, the zero-sequence voltage, v_{ZS}, defined by the summation of three-phase line-to-neutral voltages, can be derived by

$$\begin{aligned} v_{ZS} &= v_{a\_NP} + v_{b\_NP} + v_{c\_NP} = (v_a + v_b + v_c) - 3v_{NP} \\ &= R_s\,(i_a + i_b + i_c) + L_s\left(\frac{di_a}{dt} + \frac{di_b}{dt} + \frac{di_c}{dt}\right) \\ &\quad + j\omega_e\left(\lambda_{pma} + \lambda_{pmb} + \lambda_{pmc}\right) \end{aligned} \tag{5}$$

In (5), the summation of $(i_a + i_b + i_c)$ and $(di_a/dt + di_b/dt + di_c/dt)$ must be zero for the three-phase balanced drive. It is noted that $(\lambda_{pma} + \lambda_{pmb} + \lambda_{pmc})$ might not be zero if the flux saturation occurs in a machine. As reported in [20] and [21], the saturation distorts the sine-wave flux distribution to the trapezoidal-wave flux. Besides the fundamental harmonic, additional harmonics, e.g. 3rd, 6th, 9th-order etc., are induced in the phase flux. Under this effect, the summation of $(\lambda_{pma} + \lambda_{pmb} + \lambda_{pmc})$ is given by

$$\begin{aligned} &\left(\lambda_{pma} + \lambda_{pmb} + \lambda_{pmc}\right) \\ &\quad = \left|\lambda_{mag}\right| \{[k_3\cos(3\omega_e t) + k_3\cos(3\omega_e t + 2\pi) \\ &\qquad + k_3\cos(3\omega_e t + 4\pi)] + \ldots\} \\ &\quad \approx 3\left|\lambda_{mag}\right| k_3\cos(3\omega_e t) \end{aligned} \tag{6}$$

where k_3 is a fractional number proportional to the saturation condition and $|\lambda_{mag}|$ is the magnitude of fundamental flux harmonic. It is noteworthy that the third-order flux harmonic is dominant among these secondary harmonics because the magnitudes of high-order harmonics are inversely proportional to their harmonic orders.

On the other hand, variable frequency drives always use the space-vector pulse width modulation (PWM) to fully utilize the DC bus voltage. Considering the space-vector PWM (SVPWM), the summation of $(v_a + v_b + v_c)$ is approximately equal to the summation of three injected zero-sequence voltage harmonics, v_{SVPWM}, which is given by

$$\begin{aligned} &v_a + v_b + v_c \\ &= -3v_{SVPWM} \\ &= -3\left\{\frac{v_m}{5}\cos[3(\omega_e t + \phi)] - \frac{v_m}{45}\cos[9(\omega_e t + \phi)] + \ldots.\right\} \\ &\approx -3\left(\frac{v_m}{5}\cos[3(\omega_e t + \phi)]\right) = -3v_{SV} \end{aligned} \tag{7}$$

where v_m and ϕ represents the magnitude and angle of the phase voltage, and v_{SV} is the zero-sequence voltage for the SVPWM switching control.

Substituting (6) and (7) into (5), the measured v_{NP} in a healthy machine is shown to be

$$v_{NP} = -\frac{v_m}{5}\cos[3(\omega_e t + \phi)] - j\omega_e\left|\lambda_{mag}\right| k_3\cos(3\omega_e t)\,. \tag{8}$$

As seen in (8), v_{NP} contains two third-order harmonic components. At low speed when $\omega_e \ll 0$, the third-order harmonic is primarily induced by the SVPWM control. As speed increases, the saturation component increases as well, leading to the increased third-order harmonic magnitude.

B. NP VOLTAGE IN THE MACHINE UNDER THE PHASE FAULT

Considering the phase fault in Fig. 2, there is no current in A-phase due to the open circuit. As a result, the zero-sequence voltage with A-phase fault, v_{ZS_af}, should be modified from (5) to (9).

$$\begin{aligned} v_{ZS\_af} &= v_{b\_NP} + v_{c\_NP} = (v_b + v_c) - 2v_{NP\_af} \\ &= R_s\left(i_{b\_af} + i_{c\_af}\right) + L_s\left(\frac{di_{b\_af}}{dt} + \frac{di_{c\_af}}{dt}\right) \\ &\quad + j\omega_e\left(\lambda_{pma} + \lambda_{pmb} + \lambda_{pmc}\right) \\ &= j\omega_e\left(\lambda_{pma} + \lambda_{pmb} + \lambda_{pmc}\right) \end{aligned} \tag{9}$$

where v_{NP_af}, i_{b_af} and i_{c_af} represent respectively the measured NP voltage, B-phase and C-phase current under A-phase fault. In (9), $(i_{b_f} + i_{c_f})$ and $(di_{b_f}/dt + di_{c_f}/dt)$ are zeros based on Kirchhoff's current law. Due to unbalanced voltage inputs, $(v_b + v_c)$ is proportional to the voltage magnitude v_m, which is given by

$$\begin{aligned} v_b + v_c &= v_m\cos(\omega_e t + 120^\circ + \phi) \\ &\quad + v_m\cos(\omega_e t + 240^\circ + \phi) - 2v_{SVPWM} \\ &\approx v_m\cos(\omega_e t + 180^\circ + \phi) - \frac{2}{5}v_m\cos[3(\omega_e t + \phi)]\,. \end{aligned} \tag{10}$$

Substituting (10) and (6) into (9), the NP voltage with A-phase fault, v_{NP_af}, is derived by

$$\begin{aligned} v_{NP\_af} &= \frac{v_m}{2}\cos(\omega_e t + 180^\circ + \phi) - \frac{v_m}{5}\cos[3(\omega_e t + \phi)] \\ &\quad - j\frac{3}{2}\omega_e\left|\lambda_{mag}\right| k_3\cos(3\omega_e t)\,. \end{aligned} \tag{11}$$

Comparing v_{NP_af} to healthy v_{NP} in (8), a first-order harmonic due to the open-phase fault appears where the magnitude is equal to half of voltage magnitude, v_m. For the purpose of fault detection, this first-order harmonic can be isolated for the phase fault detection. Similar results for v_{NP_bf} with B-phase fault and v_{NP_cf} with C-phase fault can be developed in (12) and (13) based on the same analysis procedure.

$$\begin{aligned} v_{NP\_bf} &= \frac{v_m}{2}\cos(\omega_e t + 300^\circ + \phi) - \frac{v_m}{5}\cos[3(\omega_e t + \phi)] \\ &\quad - j\frac{3}{2}\omega_e\left|\lambda_{mag}\right| k_3\cos(3\omega_e t) \end{aligned} \tag{12}$$

$$\begin{aligned} v_{NP\_cf} &= \frac{v_m}{2}\cos(\omega_e t + 60^\circ + \phi) - \frac{v_m}{5}\cos[3(\omega_e t + \phi)] \\ &\quad - j\frac{3}{2}\omega_e\left|\lambda_{mag}\right| k_3\cos(3\omega_e t)\,. \end{aligned} \tag{13}$$

It is noted that a resistance network can be added to remove the SVPWM zero-sequence voltage harmonic for the isolation of fault harmonic. However with the resistance network, it is not possible to identify the open-switch or open-connector fault illustrated in Fig. 2 since the differential voltage between the resistance NP and machine NP is selected

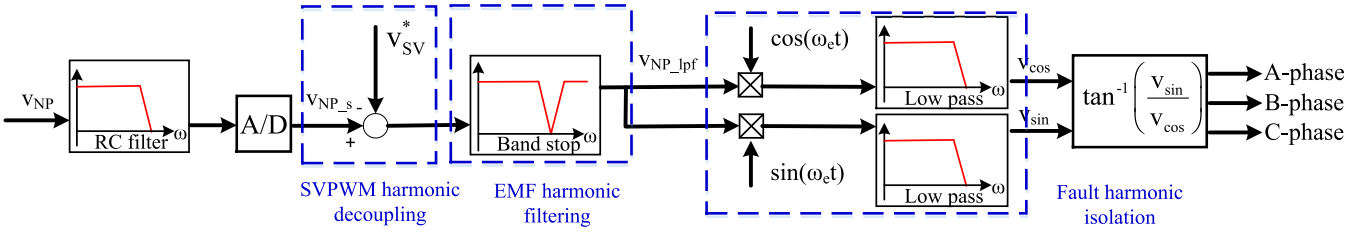

FIGURE 3. Signal process for the phase fault detection and location identification.

as the fault indicator. In this paper, the NP to ground voltage is directly measured to overcome this limitation. SVPWM harmonic will be removed based on the feedforward compensation method.

C. PHASE FAULT DETECTION BASED ON NP THE VOLTAGE HARMONIC

This part proposes the time-domain signal process to isolate the phase fault harmonic in NP voltage. Both the phase fault and location can be identified even under the drive dynamic operation.

The proposed phase fault detection is shown in Fig. 3. In general, the PWM switching harmonic is set at 10-kH∼20-kHz to achieve the dynamic operation in variable-frequency drives. Considering the PWM switching on the measured NP voltage, an analog low-pass filter (LPF) should be designed to remove the switching harmonic. In this paper, a LPF with the bandwidth at 377-Hz is used to obtain the actual NP voltage sampled into the microcontroller. Without the switching harmonic, the sampled NP voltage, v_{NP_s}, contains only the SVPWM zero-sequence voltage harmonic and the saturation harmonic, as shown in (8) assuming no phase fault appears. During the presence of phase fault, a first-order harmonic proportional to the voltage magnitude is induced, as seen from (11)-(13). For the purpose of fault detection, the first-order harmonic should be isolated.

Considering firstly the SVPWM zero-sequence voltage harmonic decoupling, a compensation voltage, v^*_{sv} in (14), can be applied.

$$v^*_{SV} = -\frac{v^*_m}{5}\cos\left[3\left(\omega_e t + \phi^*\right)\right] \tag{14}$$

where v^*_m and ϕ^* are the magnitude and angle of voltage command. In variable-frequency drives, these two variables can be easily obtained in the controller. Ideally, v^*_m is the same to the actual phase voltage output v_m in Fig. 1 assuming perfect PWM switching. However at very low speed with a low modulation factor, v_m might not be equal to v^*_m due to the nonlinear dead-time effect. The dead-time compensation technique developed in [22] should be implemented to minimize this error on v^*_m. From the experimental results in Section IV, it will be shown that the compensation voltage, v^*_{sv}, calculated by the voltage command v^*_m is accurate enough to compensate v_{sv}.

After v_{sv} decoupling, a band-stop filter (BSP) in Fig. 3 is applied to remove the flux saturation harmonic. As seen in (6), the magnitude of saturation harmonic is proportional to the machine speed, ω_e. At low speed, this saturation harmonic is sufficient low to be negligible. As a result, the bandwidth (BW) of the BSP can be designed as a speed dependent function to filter the saturation harmonic.

After removing these two harmonics, the NP voltage, denoted by v_{NP_lpf} in Fig. 3, contains only the fault induced first-order harmonic once the fault occurs. Considering the fault happened at different phases, the angle of v_{NP_af}, v_{NP_bf} and v_{NP_cf} are different, as seen in (11), (12) and (13). To identify the fault signal at different phases, the time-domain signal process is proposed by multiplying both cosine and sine functions and applying low-pass filters (LPF's) to v_{NP_lpf}, as demonstrated in Fig. 3. The corresponding fault signals for three different phases can be shown by (15), (16) and (17).

i) A-phase fault

$$\begin{aligned} v_{cos} &= \text{LPF}\left\{v_{NP\_af} \times \cos\left(\omega_e t + \phi^*\right)\right\} = -\frac{v_m}{4} \\ v_{sin} &= \text{LPF}\left\{v_{NP\_af} \times \sin\left(\omega_e t + \phi^*\right)\right\} = 0 \end{aligned} \tag{15}$$

ii) B-phase fault

$$\begin{aligned} v_{cos} &= \text{LPF}\left\{v_{NP\_bf} \times \cos\left(\omega_e t + \phi^*\right)\right\} = \frac{v_m}{8} \\ v_{sin} &= \text{LPF}\left\{v_{NP\_bf} \times \sin\left(\omega_e t + \phi^*\right)\right\} = -v_m\frac{\sqrt{3}}{8} \end{aligned} \tag{16}$$

iii) C-phase fault

$$\begin{aligned} v_{cos} &= \text{LPF}\left\{v_{NP\_cf} \times \cos\left(\omega_e t + \phi^*\right)\right\} = \frac{v_m}{8} \\ v_{sin} &= \text{LPF}\left\{v_{NP\_cf} \times \sin\left(\omega_e t + \phi^*\right)\right\} = v_m\frac{\sqrt{3}}{8} \end{aligned} \tag{17}$$

Here, v_{cos} and v_{sin} are two proposed fault signals to detect the phase fault. Table 1 summarizes v_{cos}, v_{sin} and atan2(v_{sin}/v_{cos}) under four different fault conditions: health, A-phase fault, B-phase fault and C-phase fault. It is noted that both v_{cos} and v_{sin} are proportional to the voltage magnitude, v_m. For the drive at initial state without v_m, the signal injection technique shown in [23] can be applied for the phase fault detection.

In Table 1, the function of atan2(v_{sin}/v_{cos}) is proposed to find the phase fault location. Because atan2(v_{sin}/v_{cos}) is independent on v_m at different operating conditions, the fault location can easily identify based on the angle on atan2(v_{sin}/v_{cos}).

TABLE 1. Fault signals at different fault conditions.

Fault Conditions	V_{cos}	V_{sin}	atan2(V_{sin}/V_{cos})
Health	0	0	0 ~ 360-deg
A-phase fault	$-v_m/4$	0	180-deg
B-phase fault	$v_m/8$	$-v_m\sqrt{3}/8$	300-deg
C-phase fault	$v_m/8$	$v_m\sqrt{3}/8$	60-deg

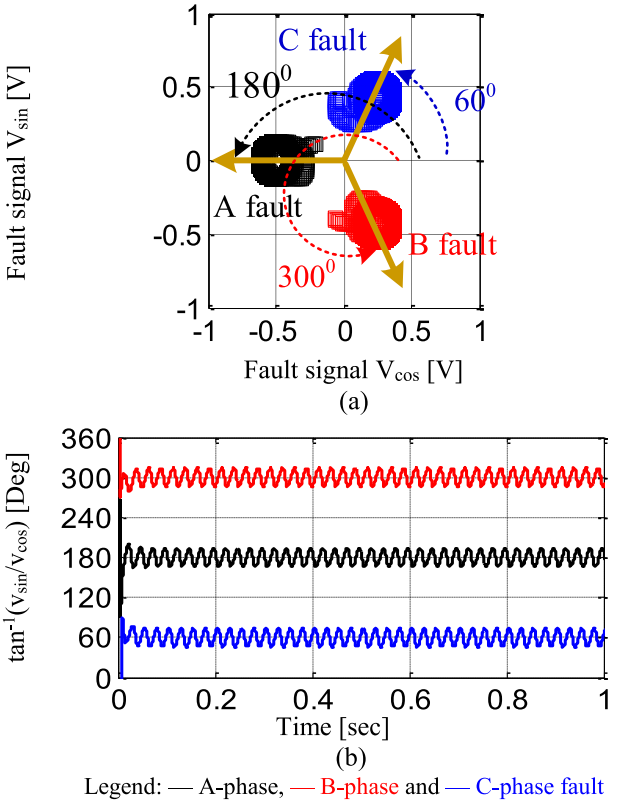

FIGURE 4. Illustration of fault signal distributions: (a) fault signal V_{cos} versus V_{sin} and (b) atan2(v_{sin}/v_{cos}) (simulation results where v_m = 1-V, $\omega_e = 2\pi \times$ 20-Hz, and LPF BW = 10-Hz).

Figure 4 simulates (a) v_{sin} versus v_{cos}, and (b) atan2(v_{sin}/v_{cos}) versus time at v_m = 1-V and $\omega_e = 2\pi \times$ 20-Hz under different phase fault conditions. The BW of LPF is designed at 10-Hz. A low rotor frequency of 20-Hz is selected to evaluate the fault detection performance at low speed. As shown in Fig. 4(a), the fault signature of v_{sin} versus v_{cos} primarily locates at the left half plane of horizontal axis under A-phase fault. Besides in (b), atan2(v_{sin}/v_{cos}) converges to 180-deg with a certain amount of time once A-phase fault occurs. Similarly results of 300-deg and 60-deg are observed with B- and C-phase fault, respectively. It is noteworthy that for the healthy condition, atan2(v_{sin}/v_{cos}) is not able to converge because v_{cos} and v_{sin} are all zeros, as shown in Table 1. However in the actual implementation, there should be a certain amount of noise in these two signals. Thus, atan(v_{sin}/v_{cos}) should result in the significant angle variation between 0-deg∼360-deg. Detailed experimental verification will be demonstrated in Section IV.

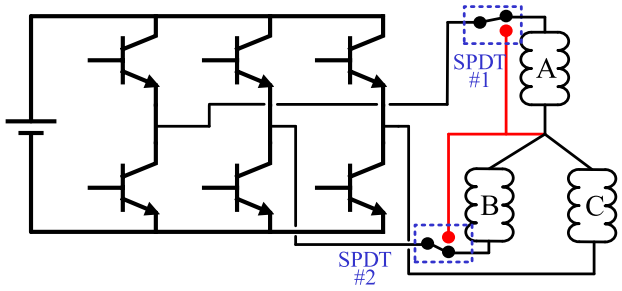

FIGURE 5. Proposed open-phase fault tolerant machine control.

TABLE 2. Tolerant drive switch control under different phase fault conditions.

Fault Condition	SPDT#1	SPDT#2	Single phase
A-phase	OFF	ON	C-phase
B-phase	ON	OFF	C-phase
C-phase (method#1)	ON	OFF	B-phase
C-phase (method#2)	OFF	ON	A-phase

III. PHASE FAULT TOLERANT CONTROL

This section explains the proposed fault tolerant control for the phase fault. Conventional phase fault tolerant control relies on redundant phases in existing machines or redundant switching legs in standard inverters [15]–[18]. A customized drive topology must be developed to achieve the fault tolerant capability. Considering the fault tolerant control at low cost, this paper proposes a fault tolerant control using the standard three-phase machine and the standard three-leg inverter. Once the phase fault occurs, a single-phase operating method is applied using remaining four switches in the inverter.

A. PHASE FAULT TOLERANT DRIVE SYSTEM

Figure 5 illustrates the proposed fault tolerant machine drive. On the basis, two single-pole double-throw (SPDT) switches are used to implement the single-phase machine drive once the phase fault and location is identified. As seen in Fig. 5, SPDT switch #1 is controlled to connect the NP when the phase fault appears on B-phase or C-phase. On the other hand, SPDT switch #2 can connect to NP once A-phase or C-phase is opened. Table 2 summarizes the corresponding switching control with respect to different phase fault conditions. These two SPDT's are controlled by the fault detection logic listed in Table 1. It is important to note that this fault tolerant control is implemented based on the three-leg inverter. Only two SPDT switches and the machine NP are added on the existing topology. As a result, the phase fault tolerant capability can be achieved at low cost which is useful for compression and pump applications.

Figure 6 explains the proposed single-phase tolerant control under the condition of C-phase connector open or C-phase inverter leg open. In this case, SPDT#2 is manipulated by connecting the NP to B-phase inverter leg. The single-phase drive using A-phase windings is realized using remaining four inverter switches. The machine is controlled

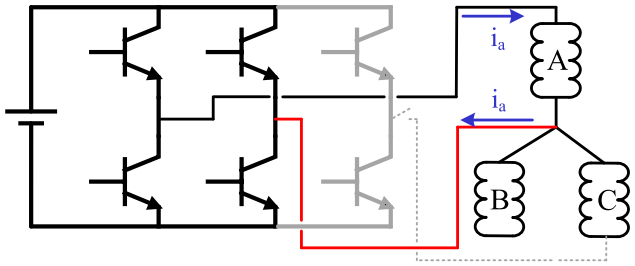

FIGURE 6. Single-phase drive under C-phase fault where SPDT#2 is ON, and SPDT#1 is OFF in Fig. 5.

based on the H-bridge PWM operation. It should be noted that the proposed tolerant control might not be able to work at zero and very low speed due to the limitation on the single-phase drive. For these applications, other systems based on the special inverter topology [15]–[18] are suggested for the fault tolerant implementation.

B. PHASE FAULT TOLERANT CONTROL OF SINGLE-PHASE DRIVE

The fault tolerant control using the single-phase drive is explained in this part. For simplicity, only the phase fault scenario in Fig. 6 is considered. Other fault conditions can be developed based on the similar analysis process.

Considering the single-phase drive in Fig. 6, the torque output T_{em_sp} should be modified by (18).

$$T_{em\_sp} = \frac{1}{3}\frac{3}{2}\frac{p}{2}\left[\lambda_{pma} \times i_a \cos(\omega_e t)\right] \tag{18}$$

where p is the machine pole pair. Compared to the three-phase drive at the normal condition, the reduced torque results due to the single-phase operation. However, the compatible power density is still achieved since the machine is provided by the same inverter power. In this paper, a voltage control method in (19) is developed for this single-phase drive once the phase fault occurs.

$$\begin{aligned} v^*_{m\_sp}&\cos\left(\theta_e + \varphi_{pf}\right) \\ &= \left|\hat{R}_s i_a + j\omega^*_e \hat{L}_s i_a + j\omega^*_e \left|\hat{\lambda}_{mag}\right| \cos\theta_e\right| \\ &= \sqrt{\left(\hat{R}_s i_a\right)^2 + \left(\omega^*_e \hat{L}_s i_a + \omega^*_e \left|\hat{\lambda}_{mag}\right| \cos\theta_e\right)^2} \end{aligned} \tag{19}$$

where $\hat{R}_s$ and $\hat{L}_s$ are the estimated resistance and inductance, $|\hat{\lambda}_{mag}|$ is the estimated flux harmonic magnitude, ω^*_e is the speed command, $v^*_{m\_sp}$ is the voltage magnitude, and φ_{pf} is the initial angle of voltage. With the voltage input of $v^*_{m\_sp}$, the speed control can be achieved based on the position feedback signal, θ_e. By using the proposed single-phase drive, closed-loop control capability can be maintained based on remaining four switches in the inverter. It is noted that the estimation errors on $\hat{R}_s$, $\hat{L}_s$ and $|\hat{\lambda}_{mag}|$ might affect $v^*_{m\_sp}$, leading to degraded torque output on the single-phase drive. However comparing to the drive in Fig. 2 without the fault tolerant control, the drive performance is improved with the closed-loop torque control. Thus, the proposed single-phase tolerant control is well-suited for safety critical automobile applications.

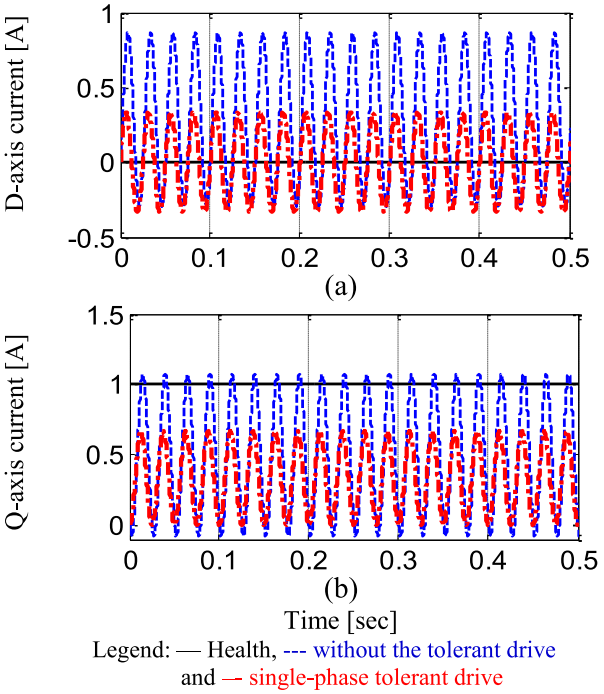

FIGURE 7. Simulation of (a) d-axis and (b) q-axis current at different faults conditions (phase current magnitude=1-A, $\omega_e = 2\pi \times 20$-Hz, R = 4.7-, and L = 4.7-mH).

Figure 7 shows simulation results of (a) rotor d-axis current, i_d, and (b) q-axis current, i_q, with and without the fault tolerant control. The phase current magnitude of 1-A is used to simulate the current response under the phase fault. In this paper, D-axis is defined to align with the rotor north pole and q-axis is 90-deg leading to d-axis. As seen in (a), current ripples in i_d are all induced in two post-fault drives once the phase fault occurs. However, current ripples are reduced if the single-phase fault tolerant drive is implemented. More importantly, a constant positive offset in i_d is observed for the normal drive with the phase fault because of unbalanced two-phase regulation. It is noteworthy that this i_d offset is disappeared for the operation of single-phase drive.

By contrast in (b), current ripples in i_q are also induced in two post-fault drives. High ripples in i_q leads to high torque ripples in a machine. For the drive without the tolerant control, a highest ripple is observed. This ripple is reduced when the single-phase drive is applied. However, the reduced torque output of 0.333 average torque is generated compared to three-phase drive. It is important to note that the safety is the primary concern once the phase fault occurs. The proposed single-phase drive is able to maintain the closed-loop control capability as well as improve the torque ripple. As soon as the phase fault is identified, secondary failures can be avoided by using the proposed single-phase drive.

IV. EXPERIMENTAL RESULTS

The proposed phase fault detection and tolerant control is experimentally evaluated on a 50-W PM machine. The

TABLE 3. Test PM machine characteristics.

Characteristics	Values
Rotor poles	8-pole
Rated torque	0.16-Nm
Rated current	1-A
Rated speed	3000-rpm (200-Hz elec frequency)
Resistance	4.7-Ω
Inductance	4.7-mH
DC bus voltage	48-V

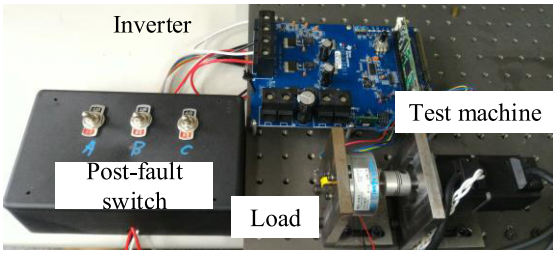

FIGURE 8. Test setup of PM machine fault detection and tolerant control.

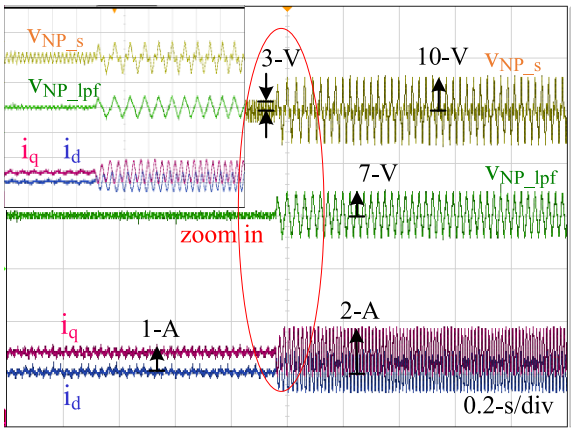

FIGURE 9. Illustration of v_{NP_s}, v_{NP_lpf}, i_d and i_q before and after A-phase fault ($\omega_e = 2\pi \times 40$-Hz, $v_m = 14$-V, and full load).

DC bus voltage is set at 48-V and the PWM frequency is 10-kHz synchronizing to the current sample frequency. All the control algorithms are implemented in a 32-bit microcontroller, TI-TMS320F28069. Machine parameters are listed in Table 3.

A. NP VOLTAGE RESPONSE UNDER THE PHASE FAULT

This part evaluates the NP voltage response under the phase fault. In this test, the machine is controlled to maintain the speed of 600-rpm ($\omega_e = 2\pi \times 40$-Hz) under load based on sensor-based FOC. The phase fault is induced based on the ON/OFF switch shown in Fig. 8. Figure 9 illustrates time domain waveforms of the sampled NP voltage and filtered NP voltage, v_{NP_s} and v_{NP_lpf} in Fig. 3, and i_d and i_q before and after the A-phase open-phase fault. Once the phase fault occurs, second-order harmonic in i_d and i_q, as well as first-order harmonics in v_{NP_s} and v_{NP_lpf} are induced. However as seen in v_{NP_s}, a third-order harmonic due to the SVPWM

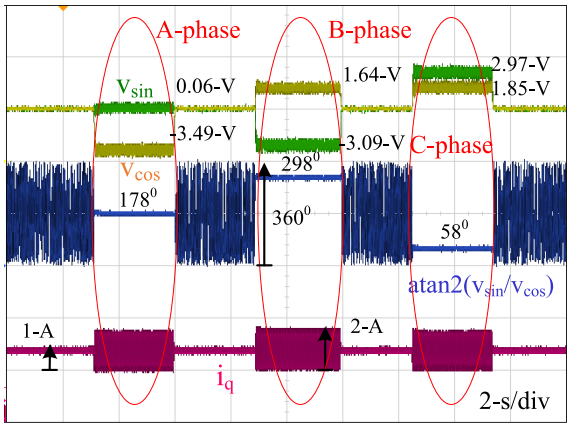

FIGURE 10. Illustration of v_{cos}, v_{sin}, atan2(v_{sin}/v_{cos}) and i_q with A-phase, B-phase and C-phase fault ($\omega_e = 2\pi \times 40$-Hz, $v_m = 14$-V, and full load).

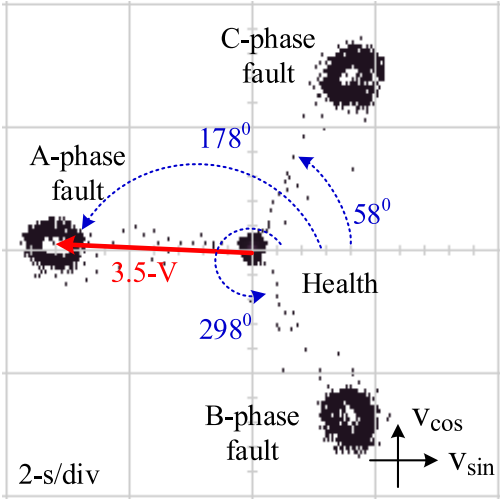

FIGURE 11. XY plot of V_{cos} versus V_{sin} under four operating fault conditions: health, A-phase, B-phase, and C-phase fault ($\omega_e = 2\pi \times 40$-Hz, $v_m = 14$-V and full load).

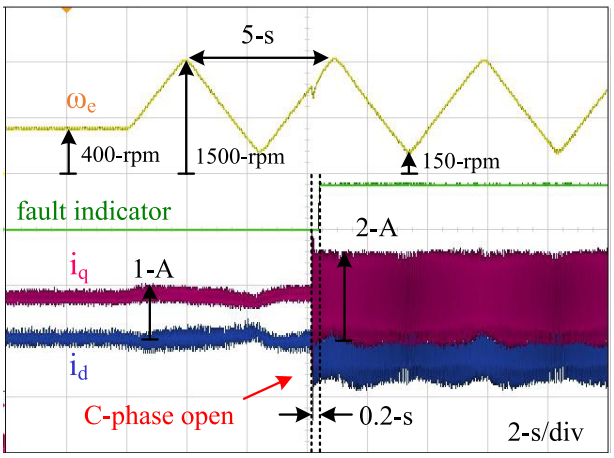

FIGURE 12. Phase fault detection during the speed transition (triangular speed command where $2\pi \times 10$-Hz $< \omega_e < 2\pi \times 50$-Hz and full load).

control is observed, resulting in the potential false positive error. By adding the feedforward voltage, v_{sv}^* in (14), the SVPWM third-order harmonic in v_{NP_s} can be removed, as

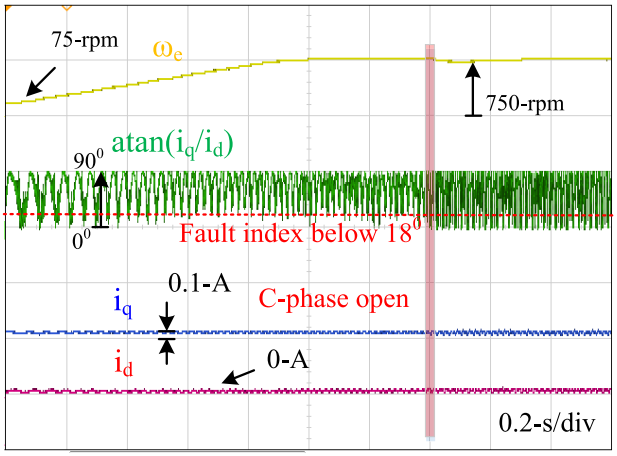

FIGURE 13. Phase fault detection at the speed of 750-rpm based on the estimation of dq current harmonics in [11] (no load condition).

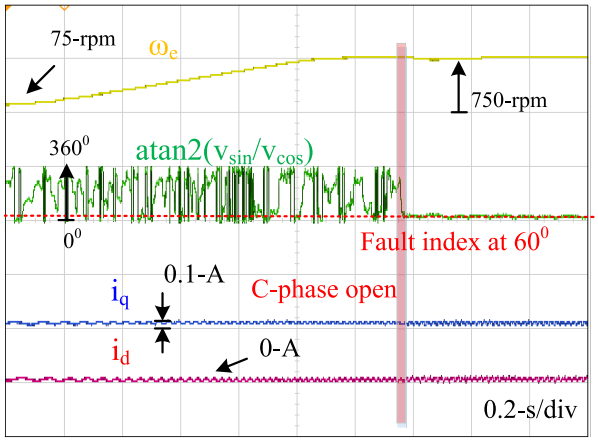

FIGURE 14. Phase fault detection at the speed of 750-rpm based on the proposed NP voltage harmonic (no load condition).

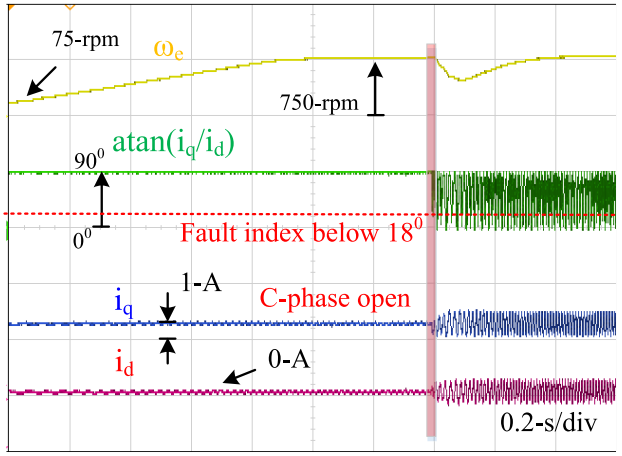

FIGURE 15. Phase fault detection at the speed of 750-rpm based on the estimation of dq current harmonics in [11] (full load condition).

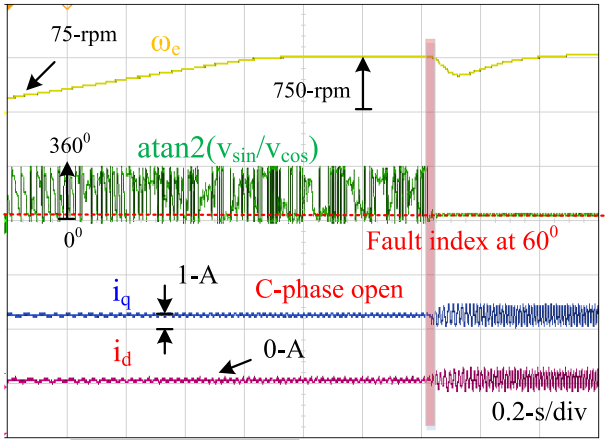

FIGURE 16. Phase fault detection at the speed of 750-rpm based on the proposed NP voltage harmonic (full load condition).

seen from v_{NP_lpf} in Fig. 9. It leads to the improved phase fault detection performance using the NP voltage.

B. FAULT DETECTION SIGNALS UNDER DIFFERENT FAULT CONDITIONS

The proposed fault detection signal listed in Table 1 is evaluated in this part. Figure 10 illustrates time-domain waveforms of v_{cos}, v_{sin}, atan2(v_{sin}/v_{cos}) and i_q by inducing A-phase, B-phase and C-phase fault sequentially. The speed and load condition is the same to the test in Fig. 9. It is shown that v_{cos} and v_{sin} converges to specific values with respect to different phase fault conditions. In addition, atan2(v_{sin}/v_{cos}) indicates the desired angles listed in Table 1 at different faults. The phase fault and the location can be identified based on these three proposed fault signals. Figure 11 further demonstrates the XY plot of v_{cos} versus v_{sin} at three different faults induced in Fig. 10. It is concluded that the phase fault location can be identified by estimating the angle of atan2(v_{sin}/v_{cos}). For example when A-phase fault occurs, atan2(v_{sin}/v_{cos}) should converge approximately to the angle of 180-deg. Compared to the simulation result in Fig. 4(a), a 2-deg error is found at the speed of 600-rpm. Nevertheless, the angle error is small enough compared to the 120-deg difference used for the identification of phase fault location. Based on these results, it is concluded that the phase fault can be detected using these three fault signals from the measurement of NP voltage.

C. PHASE FAULT DETECTION DURING SPEED TRANSIENT

This part evaluates the on-line phase fault detection performance for the speed transient operation. Figure 12 shows time-domain waveforms of ω_e, phase fault flag, i_d and i_q. In this test, a triangular speed command between 150-rpm ($\omega_e = 2\pi \times 10$-Hz) and 1500-rpm ($2\pi \times 50$-Hz) is controlled within the time period of 2-sec. The phase fault is induced during the speed change. The fault flag with the binary output (0 or 1) is determined based on three estimated fault signals shown in Fig. 10. As shown from the fault flag in Fig. 12, the phase fault is identified within the time period of 0.2-sec once the fault signals converge to desired values. In addition, no false error is demonstrated at low speed. It is concluded that the proposed fault detection is able to detect the phase fault for the dynamic operation which is typically used in variable frequency drives.

D. COMPARISON OF DIFFERENT FAULT DETECTION PERFORMANCE

At this part, the proposed fault detection using NP voltage harmonic is compared to the detection method based on the estimation of dq current harmonics developed in [11]. For the current harmonic detection, the phase fault is identified by (20).

$$\theta_{dq} = \text{atan}\left(\frac{i_q}{i_d}\right) \tag{20}$$

where i_d and i_q are d-axis and q-axis current in the rotor-referred synchronous frame, and θ_{dq} is the fault indicator. Considering a healthy machine, i_d is controlled to maintain at zero with FOC. Under this effect, θ_{dq} should be equal to 90° for the normal operation. However once a phase fault occurs, second-order harmonics are induced in both i_d and i_q, resulting in the variation on θ_{dq} from 0° to 90°. As a result, the phase fault can be found by estimating the angle of θ_{dq}. In [11], a phase fault indictor is determined once θ_{dq} is below 18°. Figure 13 demonstrates the phase fault detection based on θ_{dq} from dq current signals. The speed is controlled at 750-rpm and C-phase fault is induced. No torque load is applied to evaluate the fault detection performance at no load. In Fig. 13, both i_d and i_q are all close to zeros because no i_q is used for the torque production. Because of negligible i_q, the numerator in (20) is almost zero. The arctangent calculation is not equal to infinity, leading to the variation on θ_{dq}. Due to the limitation of small magnitude on i_q, a positive false alarm might result using dq current harmonics in [11]. By contrast, Fig. 12 shows the same fault detection where the proposed NP voltage harmonic is applied. Instead of θ_{dq}, atan2(v_{sin}/v_{cos}) in Table 1 is used for the fault detection. Because the proposed detection method is based on the measurement of voltage harmonic in NP voltage, the phase fault can be found even at no load when i_q is close to zero. Based on the comparison between Fig. 13 and 14, an improved fault detection performance is concluded on the proposed method using NP voltage harmonic.

Figures 15 and 16 compare the fault detection performance between dq current harmonics and NP voltage harmonic at full load condition. Similar to the tests in Fig. 13 and 14, the speed is at 750-rpm and C-phase is open. In Fig. 15 due to the increased i_q for the load operation, the phase fault can be detected based on θ_{dq} in (20) using dq current signals. On the other hand, a comparable fault detection performance is also achieved by estimating the NP voltage harmonic, as illustrated in Fig. 16.

E. FAULT TOLERANT CONTROL

The phase fault tolerant control performance is evaluated at this part. Figures 17 and 18 compare the drive performance with and without the proposed fault tolerant control under the phase fault. In these two tests, the speed is accelerated from 30-rpm ($\omega_e = 2\pi \times 2$-Hz) to 2000-rpm ($2\pi \times 140$-Hz) based on the FOC under the load operation. The phase fault is induced once the speed reaches 2000-rpm. Time-domain

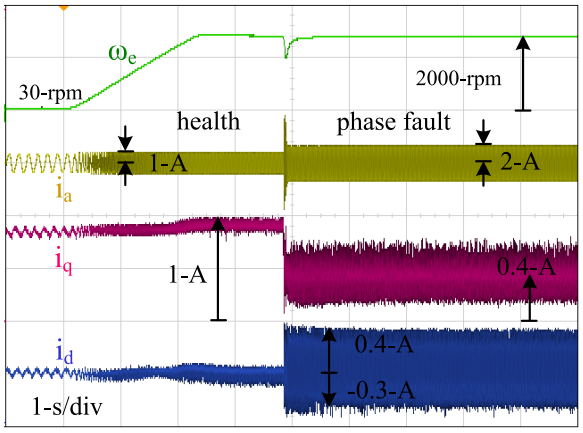

FIGURE 17. Speed closed-loop control performance when the phase fault occurs and no fault tolerant control is applied.

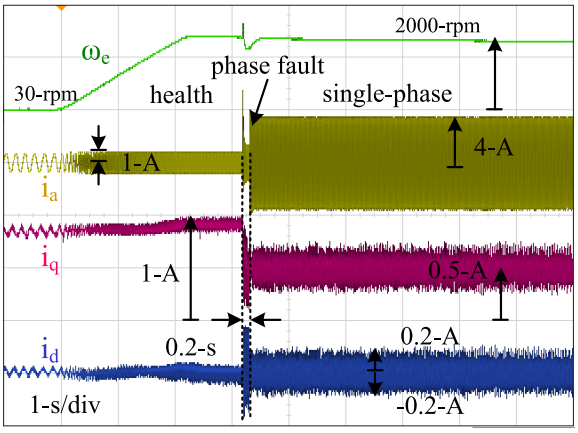

FIGURE 18. Speed closed-loop control performance when the phase fault occurs and the single-phase tolerant control is applied.

waveforms of measured speed, ω_e, A-phase current i_a, si$_d$ and i_q are saved from the scope.

As seen in Fig. 17 without the implementation of fault tolerant control, considerable ripples are observed in both i_d and i_q. In addition, a constant offset of 0.1-A in i_d is induced once the phase fault occurs. Unbalanced two-phase current regulation is the primary issue to cause the current ripple and offset. This result is consistent with the simulation in Fig. 7(a). After the presence of phase fault, secondary failures, e.g. demagnetization, might result if the drive continuously operates without the protection strategy.

By contrast for the fault tolerant control using the single-phase drive in Fig. 18, the reduced current ripples in both i_d and i_q are observed compared to the drive in Fig. 17. Because of the reduced ripple in i_q, the torque ripple decreases as well during the presence of phase fault. Although the increased phase current magnitude results, the proposed fault tolerant control can improve the drive performance using remaining inverter four switches. It is concluded that the proposed single-phase tolerant control can be implemented on compression and pump applications to increase the system reliability with low cost.

V. CONCLUSIONS

Key conclusions are summarized as follows:

- By using the proposed time-domain fault detection method, the phase fault and the location can be identified within the time period of 0.2-sec under the speed transient operation.
- The feedforward voltage, v_{sv}^{*} in (14), is sufficient to compensate the SVPWM zero-sequence voltage in the measured NP voltage for the phase fault detection.
- The phase fault is detected based on the estimation of v_{sin} and v_{cos}. The fault location is identified by the angle of atan2(v_{sin}/v_{cos}). No machine parameter is required for the proposed fault detection method.
- Based on the experimental evaluation, the proposed single-phase fault tolerant control can improve the torque ripple using remaining inverter four switches during the presence of phase fault.

REFERENCES

[1] B. Mirafzal, "Survey of fault-tolerance techniques for three-phase voltage source inverters," *IEEE Trans. Ind. Electron.*, vol. 61, no. 10, pp. 5192–5202, Oct. 2014.
[2] A. H. Bonnett and C. Yung, "Increased efficiency versus increased reliability," *IEEE Ind. Appl. Mag.*, vol. 14, no. 1, pp. 29–36, Jan. 2008.
[3] W. Sun, Y. Zhang, Y. Huang, H. Gao, and O. Kaynak, "Transient-performance-guaranteed robust adaptive control and its application to precision motion control systems," *IEEE Trans. Ind. Electron.*, vol. 63, no. 10, pp. 6510–6518, Oct. 2016.
[4] W. Sun, H. Pan, J. Yu, and H. Gao, "Reliability control for uncertain half-car active suspension systems with possible actuator faults," *IET Control Theory Appl.*, vol. 8, no. 9, pp. 746–754, Jun. 2014.
[5] J. Yao, Z. Jiao, D. Ma, and L. Yan, "High-accuracy tracking control of hydraulic rotary actuators with modeling uncertainties," *IEEE/ASME Trans. Mechatronics*, vol. 19, no. 2, pp. 633–641, Apr. 2014.
[6] A. Gandhi, T. Corrigan, and L. Parsa, "Recent advances in modeling and online detection of stator interturn faults in electrical motors," *IEEE Trans. Ind. Electron.*, vol. 58, no. 5, pp. 1564–1575, May 2011.
[7] J. O. Estima and A. J. M. Cardoso, "A new approach for real-time multiple open-circuit fault diagnosis in voltage-source inverters," *IEEE Trans. Ind. Appl.*, vol. 47, no. 6, pp. 2487–2494, Dec. 2011.
[8] H. Henao *et al.*, "Trends in fault diagnosis for electrical machines: A review of diagnostic techniques," *IEEE Ind. Electron. Mag.*, vol. 8, no. 2, pp. 31–42, Feb. 2014.
[9] A. Sapena-Bañó, M. Pineda-Sanchez, R. Puche-Panadero, J. Martinez-Roman, and D. Matić, "Fault diagnosis of rotating electrical machines in transient regime using a single stator current's FFT," *IEEE Trans. Instrum. Meas.*, vol. 64, no. 11, pp. 3137–3146, Nov. 2015.
[10] A. Kontarcek, P. Bajec, M. Nemec, V. Ambrozic, and D. Nedeljkovic, "Cost-effective three-phase PMSM drive tolerant to open-phase fault," *IEEE Trans. Ind. Electron.*, vol. 62, no. 11, pp. 6708–6718, Nov. 2015.
[11] S. S. Kuruppu and N. A. Kulatunga, "D-Q current signature-based faulted phase localization for SM-PMAC machine drives," *IEEE Trans. Ind. Electron.*, vol. 62, no. 1, pp. 113–121, Jan. 2015.
[12] A. Kontarcek, P. Bajec, M. Nemec, V. Ambrozic, and D. Nedeljkovic, "Cost-effective three-phase PMSM drive tolerant to open-phase fault," *IEEE Trans. Ind. Electron.*, vol. 62, no. 11, pp. 6708–6718, Nov. 2015.
[13] J. O. Estima and A. J. M. Cardoso, "A new algorithm for real-time multiple open-circuit fault diagnosis in voltage-fed PWM motor drives by the reference current errors," *IEEE Trans. Ind. Electron.*, vol. 60, no. 8, pp. 3496–3505, Sep. 2013.
[14] W.-S. Im, J.-M. Kim, D.-C. Lee, and K.-B. Lee, "Diagnosis and fault-tolerant control of three-phase ACâĂŞDC PWM converter systems," *IEEE Trans. Ind. Appl.*, vol. 49, no. 4, pp. 1539–1547, Mar. 2013.
[15] A. Gaeta, G. Scelba, and A. Consoli, "Modeling and control of three-phase PMSMs under open-phase fault," *IEEE Trans. Ind. Appl.*, vol. 49, no. 1, pp. 74–83, Jan. 2013.
[16] M. Naidu, S. Gopalakrishnan, and T. W. Nehl, "Fault-tolerant permanent magnet motor drive topologies for automotive X-by-wire systems," *IEEE Trans. Ind. Appl.*, vol. 46, no. 2, pp. 841–848, Feb. 2010.
[17] S. Bolognani, M. Zordan, and M. Zigliotto, "Experimental fault-tolerant control of a PMSM drive," *IEEE Trans. Ind. Electron.*, vol. 47, no. 5, pp. 1134–1141, May 2000.
[18] Y. Song and B. Wang, "Analysis and experimental verification of a fault-tolerant HEV powertrain," *IEEE Trans. Power Electron.*, vol. 28, no. 12, pp. 5854–5864, Dec. 2013.
[19] B. A. Welchko, T. A. Lipo, T. M. Jahns, and S. E. Schulz, "Fault tolerant three-phase AC motor drive topologies: A comparison of features, cost, and limitations," *IEEE Trans. Power Electron.*, vol. 19, no. 4, pp. 1108–1116, Jul. 2004.
[20] C. Cui, G. Liu, K. Wang, and X. Song, "Sensorless drive for high-speed brushless DC motor based on the virtual neutral voltage," *IEEE Trans. Power Electron.*, vol. 30, no. 6, pp. 3275–3285, Jun. 2015.
[21] J. X. Shen, Z. Q. Zhu, and D. Howe, "Sensorless flux-weakening control of permanent-magnet brushless machines using third harmonic back EMF," *IEEE Trans. Ind. Appl.*, vol. 40, no. 6, pp. 1629–1636, Nov. 2004.
[22] J.-W. Choi and S.-K. Sul, "Inverter output voltage synthesis using novel dead time compensation," *IEEE Trans. Power Electron.*, vol. 11, no. 2, pp. 221–227, May 1996.
[23] F. Briz, M. W. Degner, P. García, and A. B. Diez, "High-frequency carrier-signal voltage selection for stator winding fault diagnosis in inverter-fed AC machines," *IEEE Trans. Ind. Electron.*, vol. 55, no. 12, pp. 4181–4190, Dec. 2008.

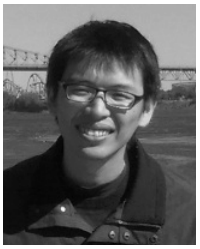

SHIH-CHIN YANG (S'10–M'12) was born in Taiwan. He received the M.S. degree in mechanical engineering from National Taiwan University, Taiwan, in 2007, and the Ph.D. degree in mechanical engineering from the University of Wisconsin-Madison, WI, USA, in 2011.

From 2011 to 2015, he was a Research Engineer with the Texas Instruments Motor Laboratory, Dallas, TX, USA. He is currently an Assistant Professor with National Taiwan University, Taiwan, responsible for developing motor drive and motor control technology. His research interests include motor drive, power electronics, and control systems.

Prof. Yang received the IEEE Industry Applications Society Industrial Drive Committee First Prize Paper Award in 2011.

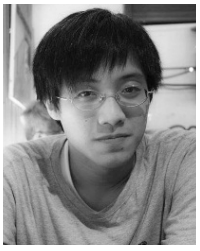

GUAN-REN CHEN (S'17) was born in Taiwan. He received the M.S. degree in opto-mechatronics engineering from National Central University, Taiwan, in 2014. He is currently pursuing the Ph.D. degree in mechanical engineering with National Taiwan University.

His current research interests include control systems, motor drives, and intelligent vehicles.

DA-REN JIAN was born in Taiwan. He received the B.S. degree in mechanical engineering from the National Taipei University of Technology, Taipei City, Taiwan, in 2015. He is currently pursuing the M.S. degree in mechanical engineering with National Taiwan University, Taiwan.

His research interests include permanent magnet machine drive, fault detection, and fault tolerant control.